

Supporting Information

Influence of dopant size and electron affinity on the electrical conductivity and thermoelectric properties of a series of conjugated polymers

Zhiming Liang^a, Yadong Zhang^b, Maryam Souric, Xuyi Luo^d, Alex M. Boehm^a, Ruipeng Li^e, Yan Zhang^a, Tairan Wang^f, Doo-Young Kim^a, Jianguo Mei^d, Seth R. Marder^b, Kenneth R. Graham^{*a}

^aDepartment of Chemistry, University of Kentucky, Lexington, Kentucky 40506, USA
School of Chemistry and Biochemistry and Center for Organic Photonics and Electronics,

^bGeorgia Institute of Technology, Atlanta, Georgia 30332, USA

^cDepartment of Physics, University of Kentucky, Lexington, Kentucky 40506, USA

^dDepartment of Chemistry, Purdue University, West Lafayette, Indiana 47907, United States

^eBrookhaven National Laboratory, Shirley, New York 11967, USA

^fSchool of Physics and Telecommunication, South China Normal University, Guangzhou 510000, P.R. China

*E-mail: kenneth.graham@uky.edu

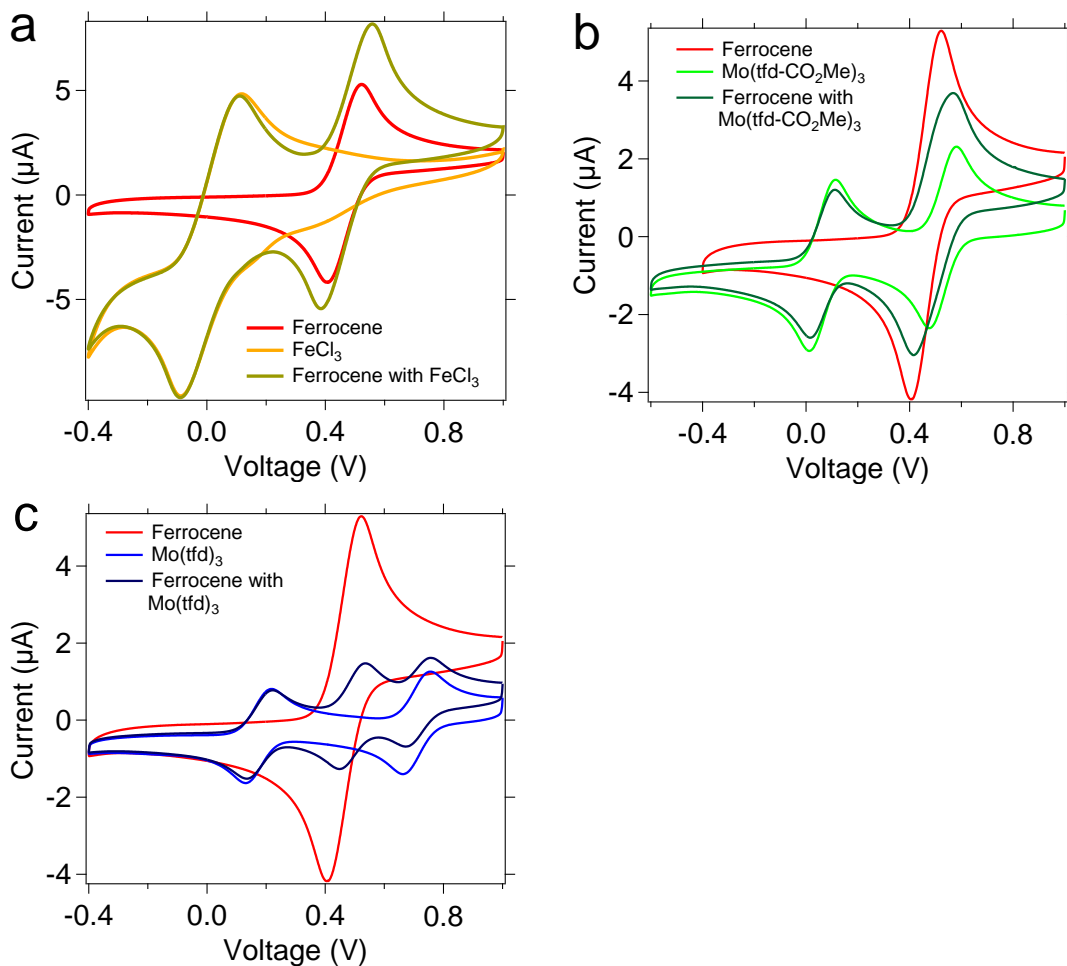


Figure S1: CV of polymers and dopants. a) FeCl_3 and ferrocene, b) $\text{Mo}(\text{tfdCO}_2\text{Me})_3$ and ferrocene, c) $\text{Mo}(\text{tfd})_3$ and ferrocene.

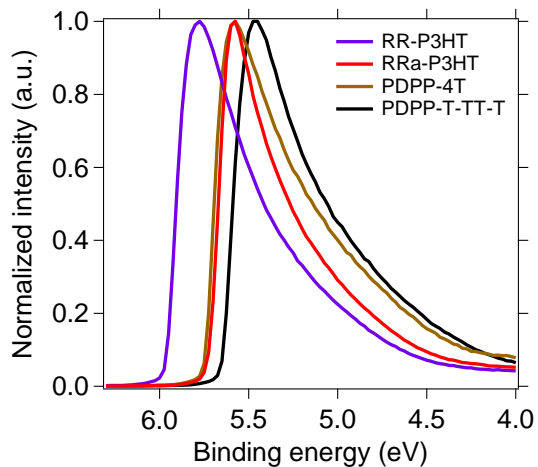


Figure S2: UPS spectra of the SECO region of the polymers.

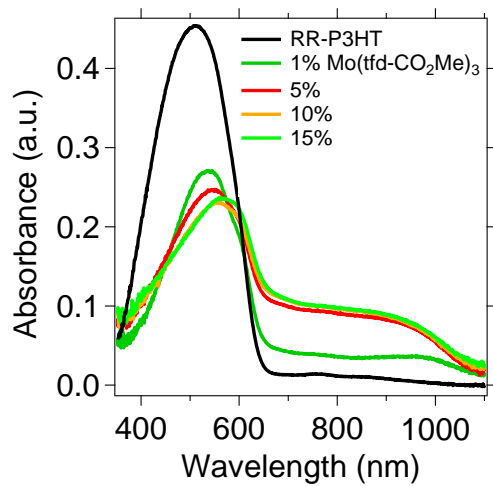


Figure S3: UV-Vis absorbance of Mo(tfdCO₂Me)₃ single-solution doped RR-P3HT.

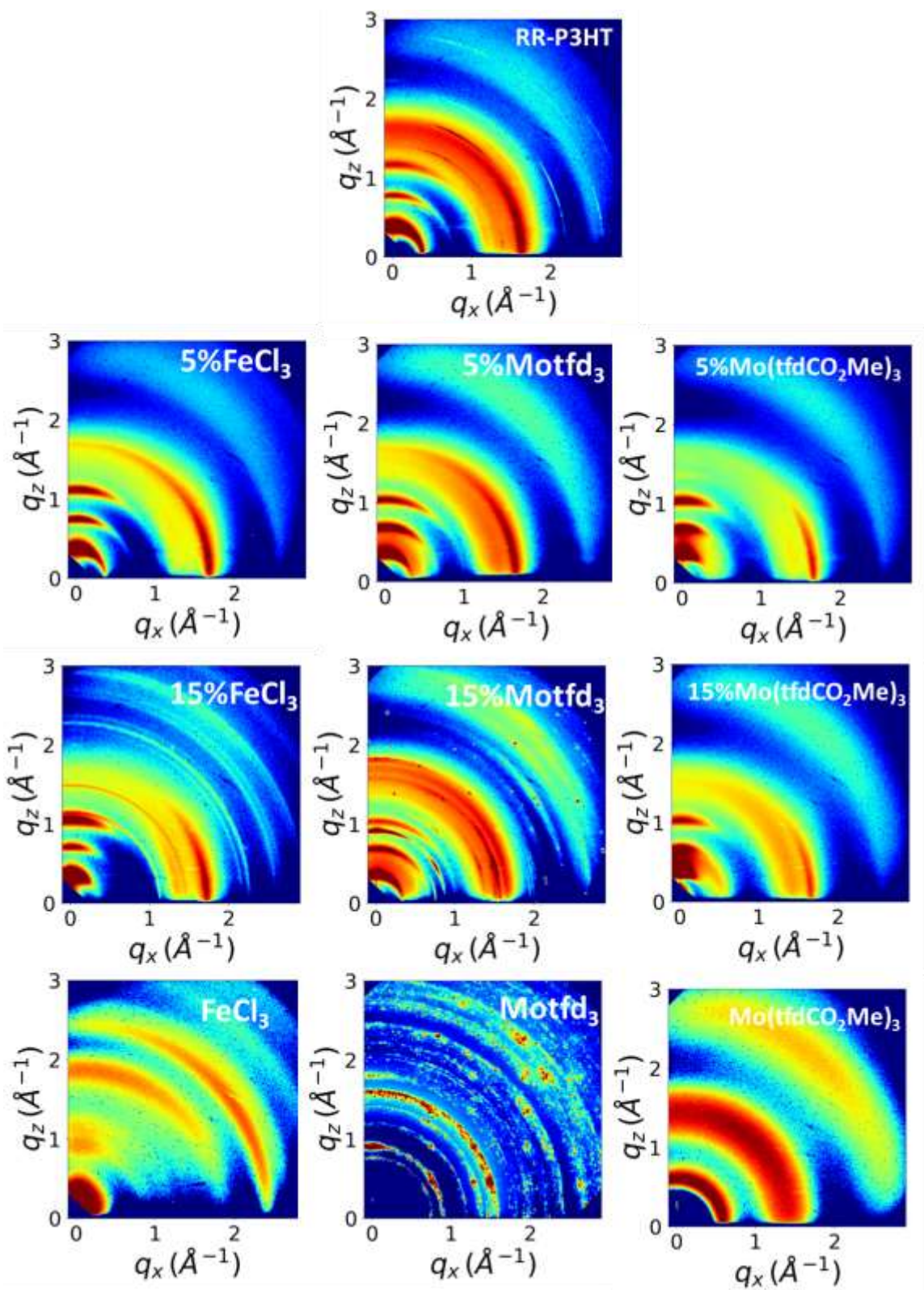


Figure S4: GIWAXS of dopants, RR P3HT and single-solution doped RR P3HT.

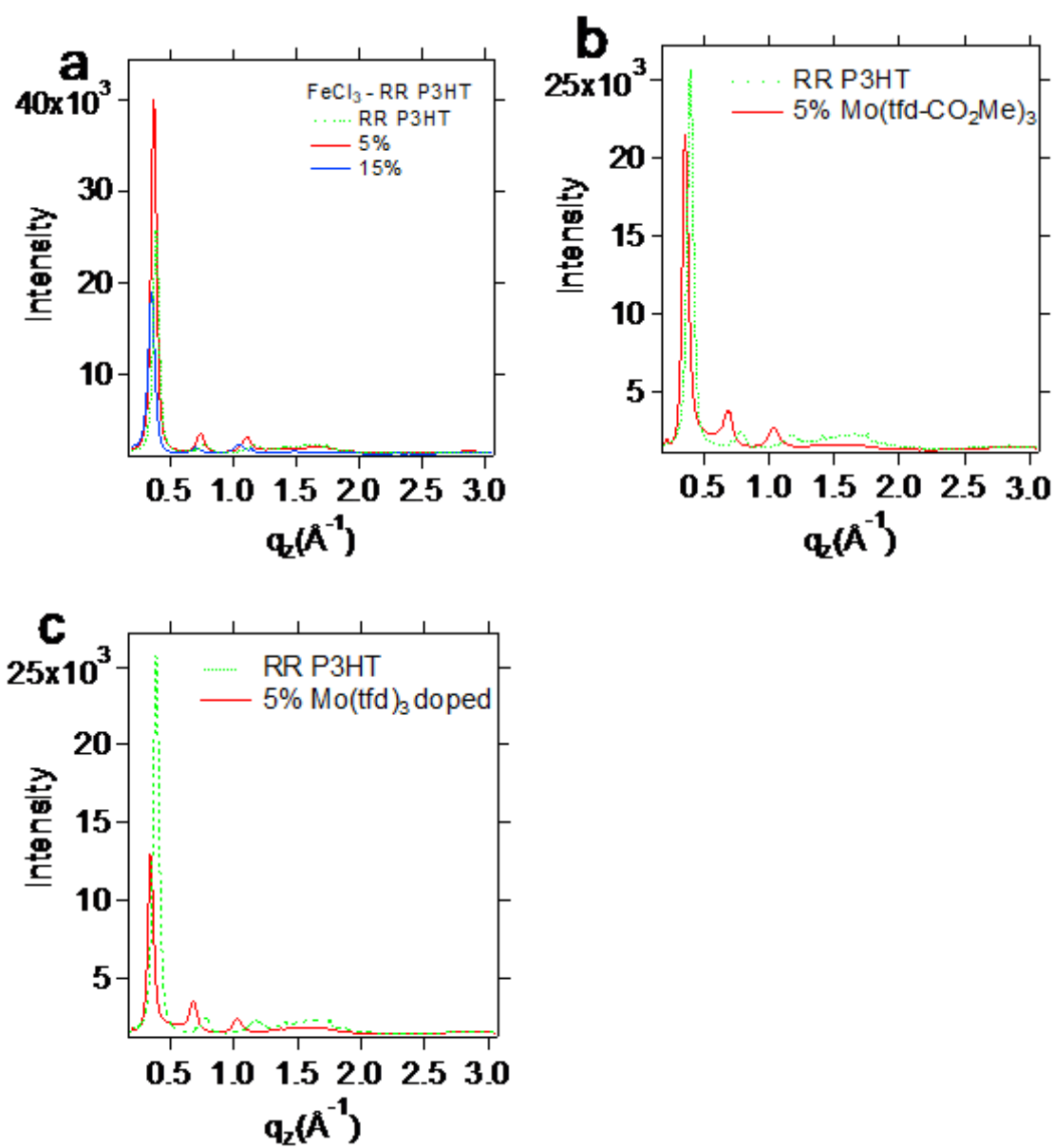


Figure S5: GIWAXS of single-solution doped RR-P3HT. (out of plane integrated intensity over 60 – 90 degree cake slice)

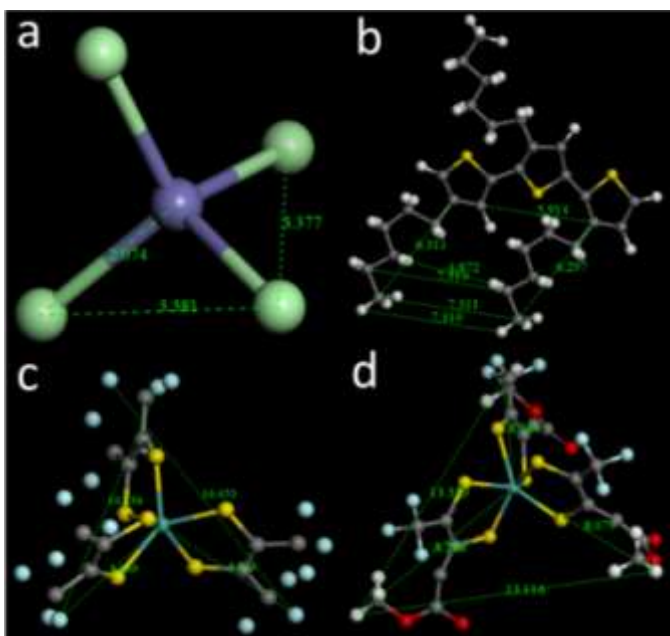
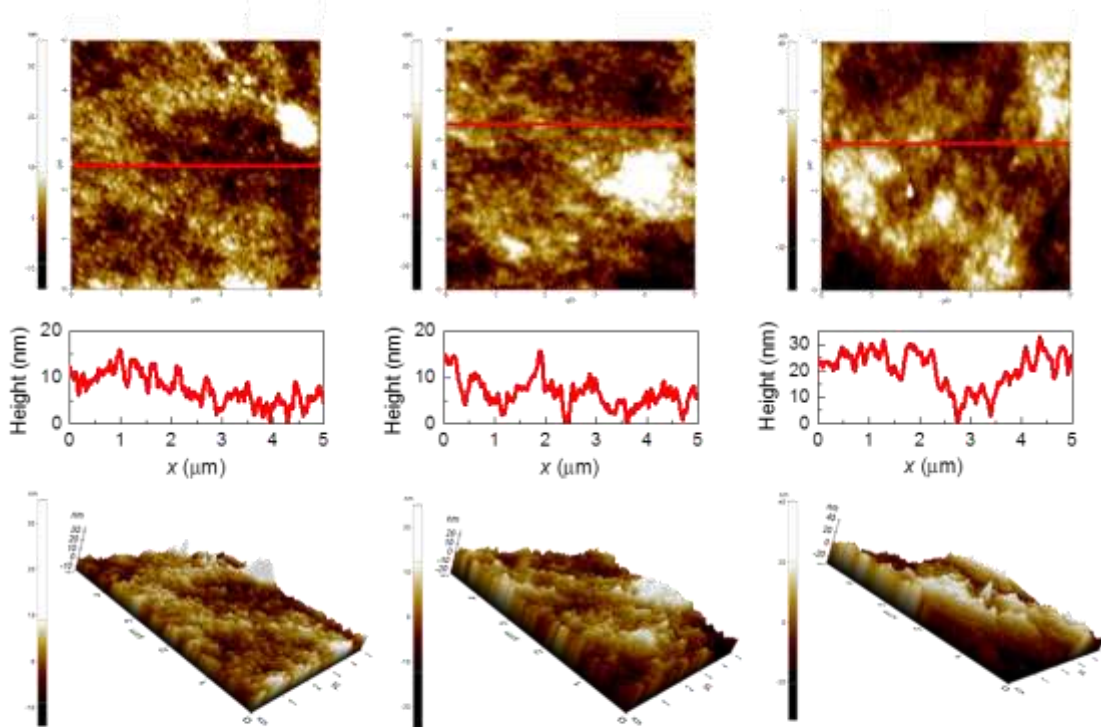


Figure S6: Chemical structure of dopants. a) FeCl_4^- , b) three repeating units of P3HT, c) $\text{Mo}(\text{tfd})_3$, and d) $\text{Mo}(\text{tfd}-\text{CO}_2\text{Me})_3$. These structures are geometry optimized by *ab initio* code Dmol3 in Materials studio. LDA (local density approximation) is chosen as the approximation to the exchange and correlation energy functional. SCF (Self-consistent field) tolerance is 1.0×10^{-6} Ha. These optimized values are comparable to some similar X-ray structure in the references)^{1,2}



Mo(tfd)₃ Rq(nm) = 4.586 Mo(tfdCO₂Me)₃ Rq(nm) = 6.285 FeCl₃ Rq(nm) = 10.418

Figure S7: AFM images of 5% molar fraction FeCl₃, Mo(tfd)₃, and Mo(tfdCO₂Me)₃ single-solution doped RR P3HT.

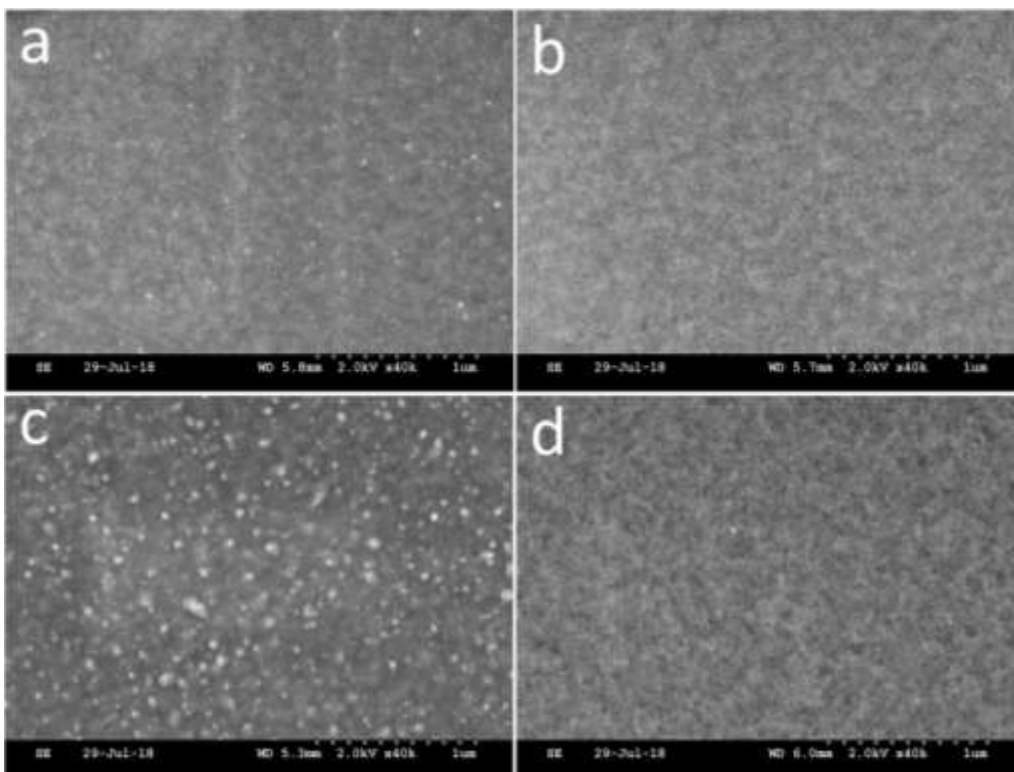


Figure S8: SEM images of doped RR-P3HT. a) 5% FeCl₃, b) 5% Mo(tfd)₃, c) 15% FeCl₃, b) 15% Mo(tfd)₃.

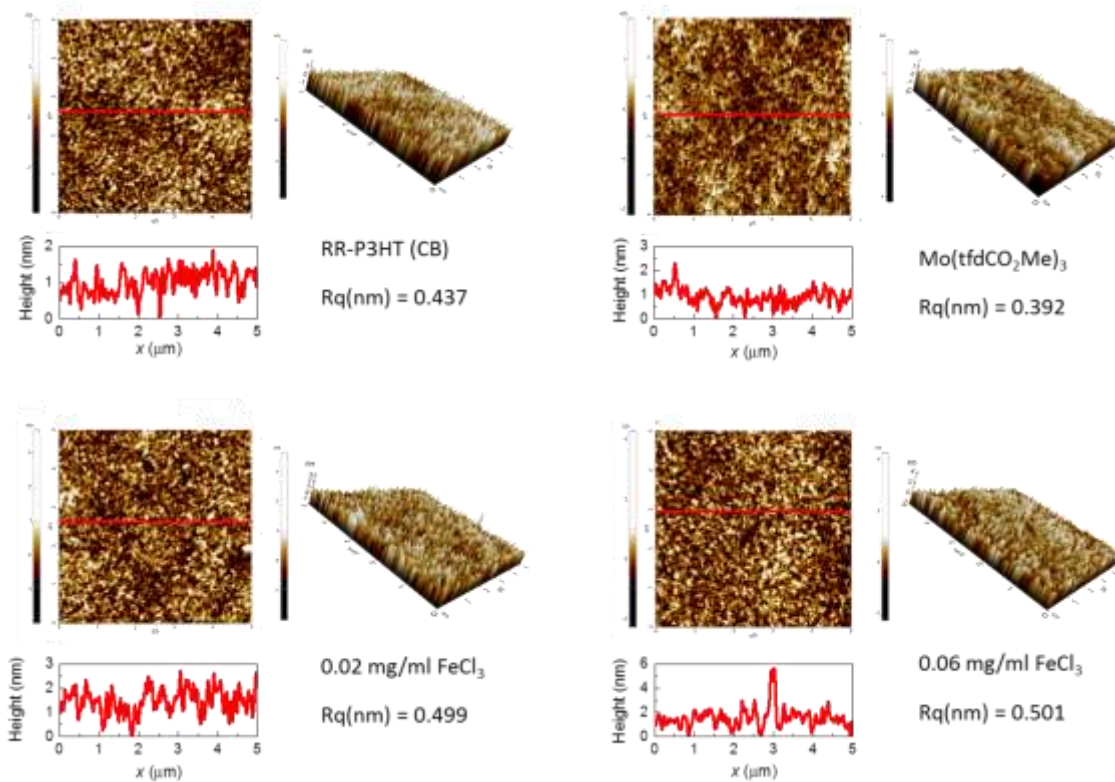


Figure S9: AFM images of sequential processing FeCl_3 , and $\text{Mo}(\text{tfd-CO}_2\text{Me})_3$ doped RR-P3HT.

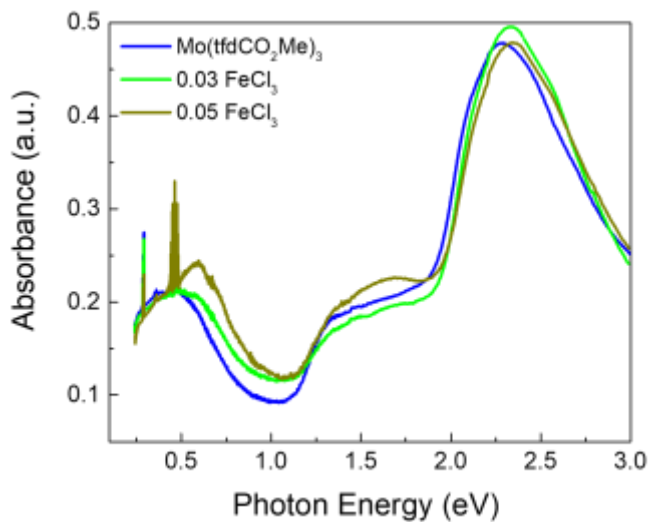


Figure S10. UV-Vis-IR absorbance spectra of sequentially doped RR-P3HT.

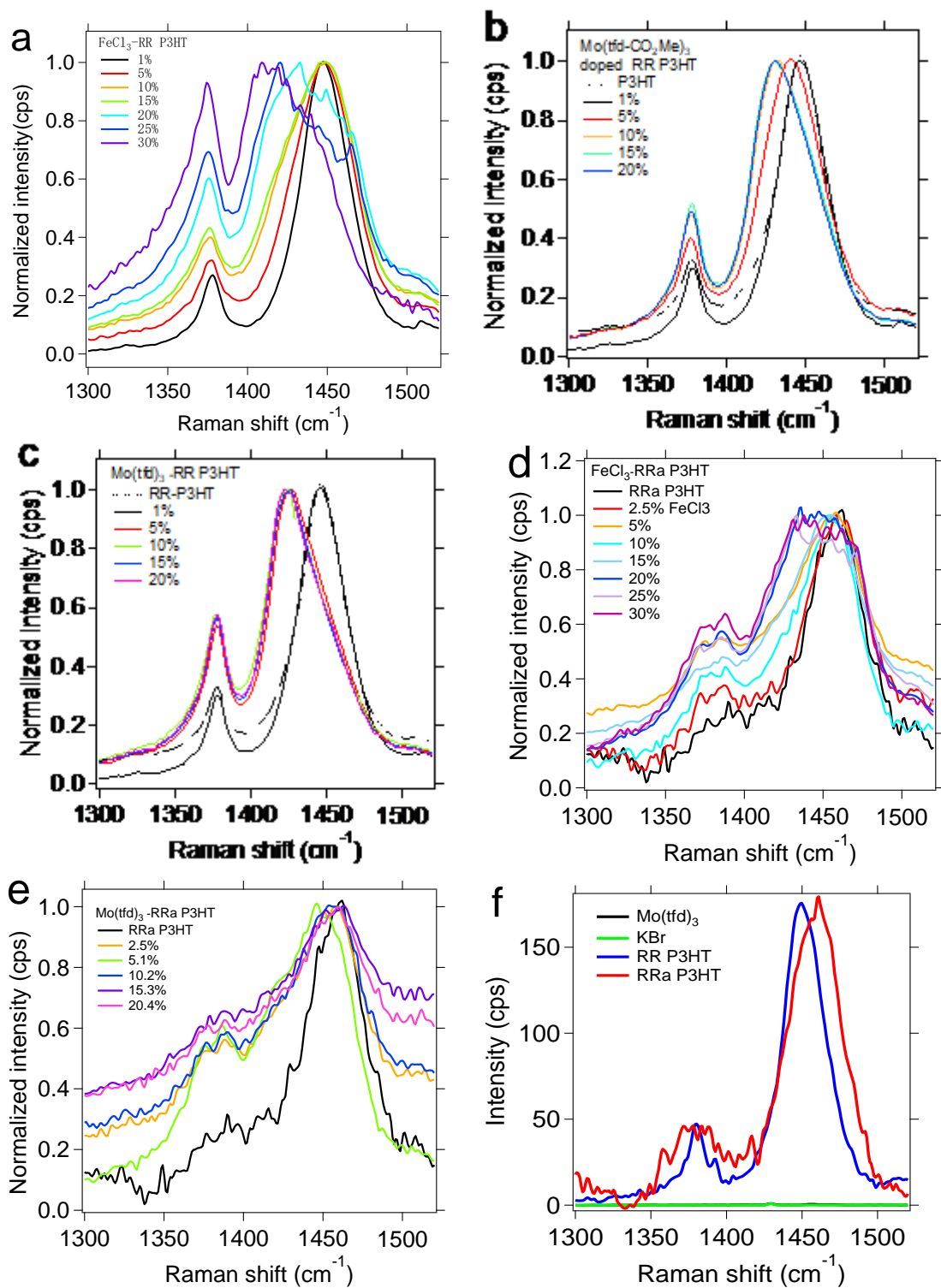
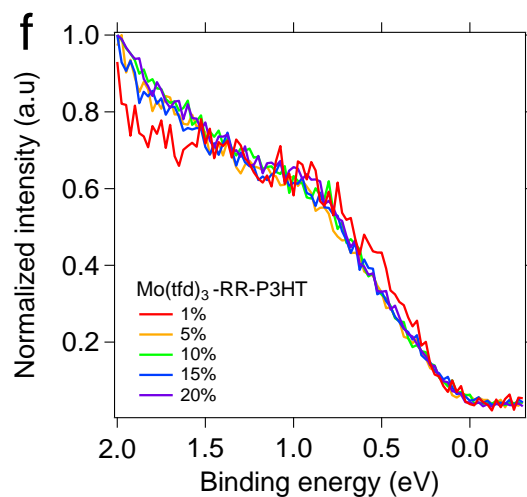
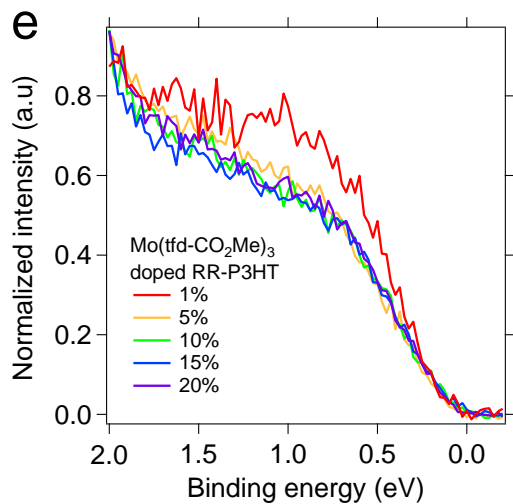
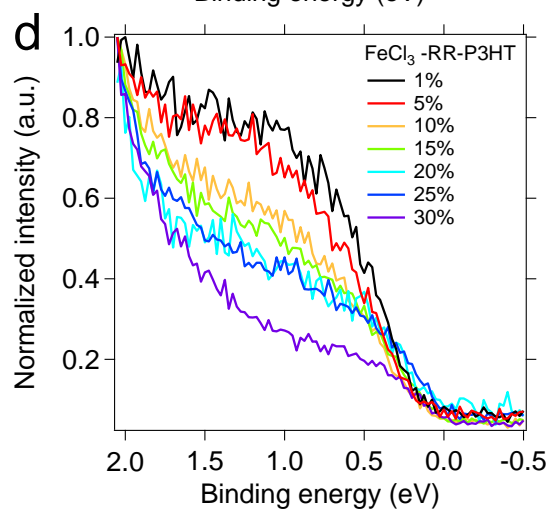
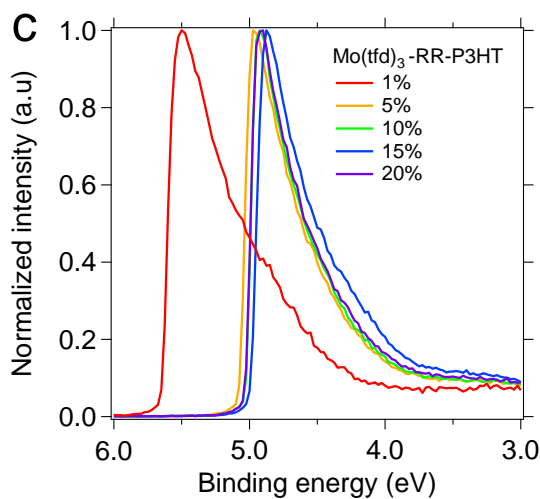
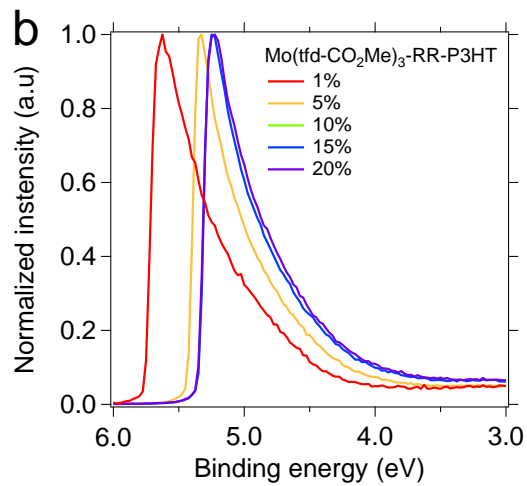
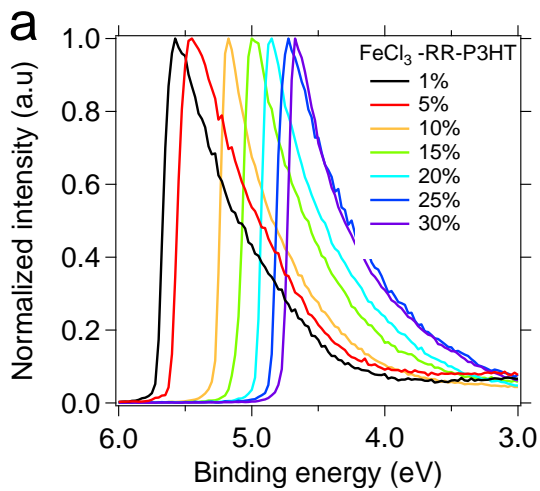


Figure S11. Raman spectra (532 nm Laser)(single-solution doped): a) FeCl_3 -RR P3HT, b) $\text{Mo}(\text{tfdCO}_2\text{Me})_3$ -RR P3HT, c) $\text{Mo}(\text{tfd})_3$ -RR P3HT, d) FeCl_3 -RRa P3HT, e) $\text{Mo}(\text{tfd})_3$ -RRa P3HT, f) RR, RRa P3HT, and $\text{Mo}(\text{tfd})_3$.



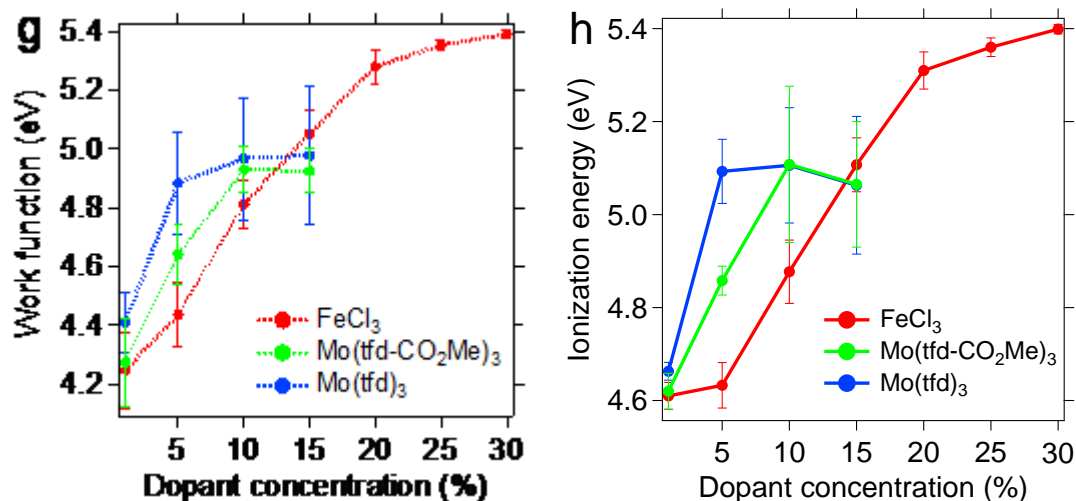


Figure S12: SECO and HOMO onset of FeCl₃(a,d), Mo(tfdCO₂Me)₃ (b,e), and Mo(tfd)₃ (c,f) single-solution doped RR-P3HT; Summarized Work function (g),and IE (h).

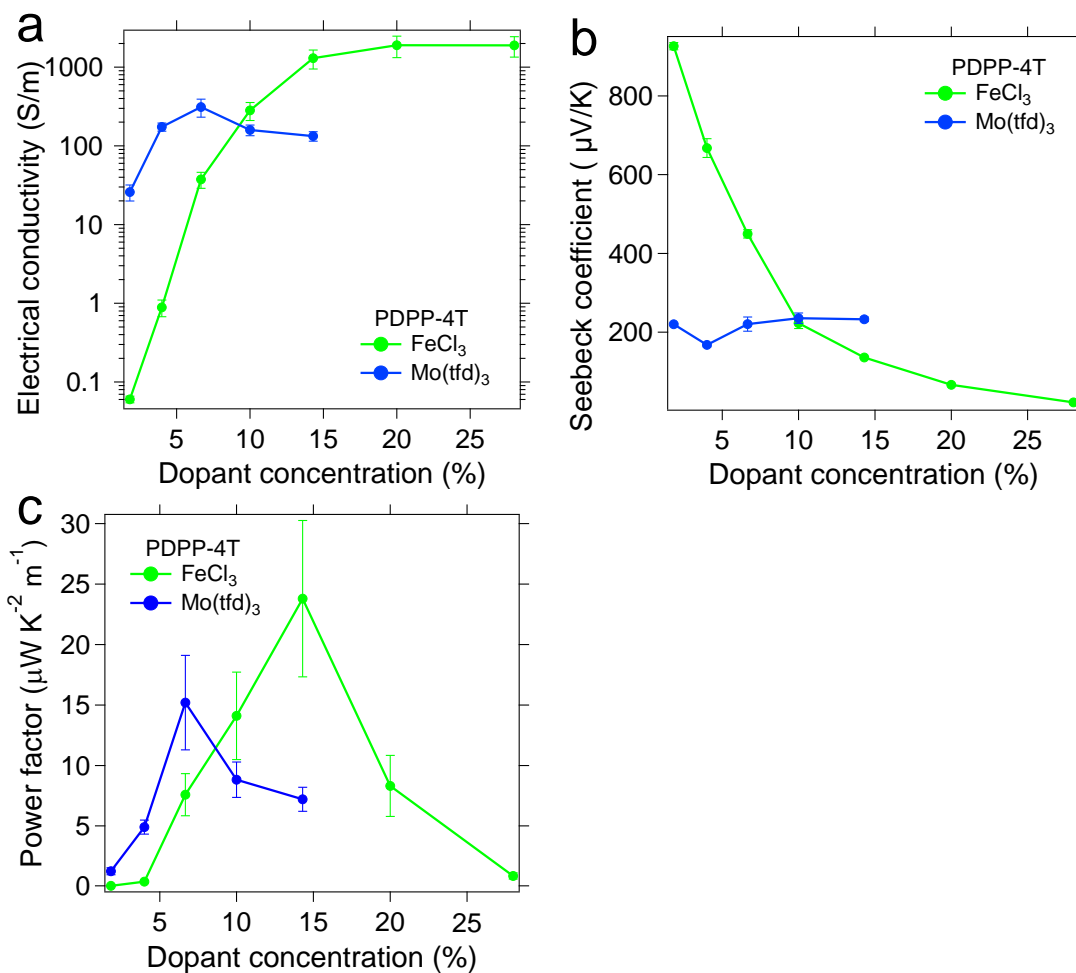


Figure S13. Electrical conductivity vs. dopant concentration (a), Seebeck coefficient vs. dopant concentration (b), and power factor vs. dopant concentration (c) for solution processing doped PDPP-4T with Mo(tfd)₃, and FeCl₃.

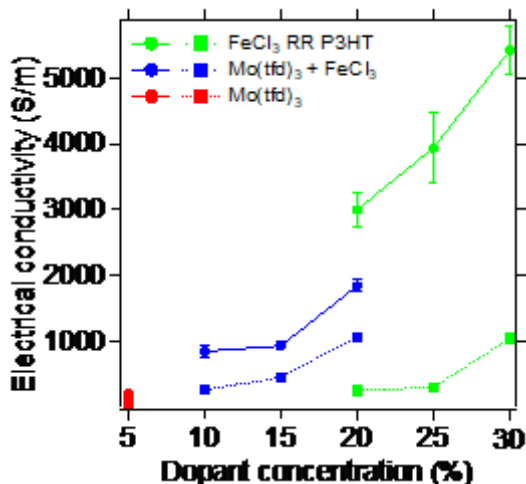


Figure S14. Electrical conductivity of RR-P3HT films produced from a single-solution with Mo(tfd)₃, FeCl₃, and both 5% Mo(tfd)₃ and FeCl₃ combined measured immediately after removal from the nitrogen filled glovebox (solid line) and after storage in ambient air for 4 months (dotted lines).

Experimental Section:

Materials. RR-P3HT and RRa-P3HT(Rieke metals); iron(III) chloride (anhydrous, 98%, crystalline, Alfa Aesar); chloroform (Anhydrous, DriSolv); acetonitrile (>99.5%, Sigma-aldrich); chlorobenzene (Anhydrous, DriSolv); bismuth (99.99%, Kurt J.Lesker). Mo(tfd)₃ and Mo(tfdCO₂Me)₃ was synthesized as reported in previous publications.^{3,4} The synthesis of PDPP-4T and PDPP-T-TT-T also followed the previously reported procedures.^{5,6}

Film preparation and doping.

Single-Solution processing:

P3HT was dissolved in chloroform with a concentration of 15 mg/ml; PDPP-4T, PDPP-T-TT-T, FeCl₃, and Mo(tfdCO₂Me)₃ were dissolved in chloroform with a concentration

of 5 mg/ml; and Mo(tfd)₃ was dissolved in chloroform at 3 mg/ml. The doped solutions were stirred on a hotplate at 40 °C for 10 hours before the films were fabricated by drop-casting the solutions onto glass substrates. Films thicknesses ranged from 2 to 4 μm. All steps were completed in a nitrogen filled glovebox with H₂O < 0.1ppm, and O₂ < 0.1 ppm.

Sequential processing doping:

RR-P3HT was dissolved in chlorobenzene with a concentration of 15 mg/ml; FeCl₃, and Mo(tfdCO₂Me)₃ were dissolved in acetonitrile at 5 mg/ml. RR-P3HT was spin-cast at 3000 rpm for 30 seconds; then FeCl₃, or Mo(tfdCO₂Me)₃ solutions were dropped on top of the RR-P3HT films and let sit for 10 seconds before spinning off the dopant solution at 3000 rpm for 30 seconds. Films thicknesses ranged from 40 to 60 nm. All steps were carried out in a nitrogen filled glovebox with H₂O < 0.1ppm, and O₂ < 0.1 ppm.

Film characterization.

UPS measurements were conducted in a PHI 5600 UHV system with an 11 inch diameter hemispherical electron energy analyzer with multichannel detector. The photon source for the UPS measurements was an Excitech H Lyman- α lamp (E-LUXTM121) coupled with a 90° ellipsoidal mirror (E-LUXTM EEM Optical Module) with a dry nitrogen purge of the beam path at 7.5 - 8.5 Torr, as detailed in a previous publication.⁷ All UPS measurements were recorded with -5V sample bias and a pass energy of 5 eV. IPES measurements were performed using the Bremsstrahlung isochromat mode with electron kinetic energies below 5 eV to minimize sample damage. The low energy electron beam was generated using a Kimball Physics ELG-2 electron gun equipped with a low temperature (1150K) BaO cathode. Emitted photons were collected and focused with a fused silica bi-convex lens into the photon detector that consisted of an optical bandpass

filter (214 nm, Andover corporation) and a photomultiplier tube (R585, Hamamatsu Photonics). The IPES measurement was performed with a custom LabVIEW program. During all IPES measurements the UHV chamber was blacked-out to exclude external light and samples were held under a -20 V bias.

Grazing incidence wide angle X-ray scattering:

GIWAXS measurements were carried out at the 11-BM Complex Materials Scattering (CMS) beamline of the National Synchrotron Light Source II (NSLS-II), Brookhaven National Laboratory. The x-ray with the wavelength of 0.0918 nm shone on the thin film samples at the incident angle of 0.15° . An in-vacuum CCD (Photonic Science) detector was tilted $\sim 19^\circ$ from the incident X-ray beam direction and located 227mm away from the samples, which were calibrated by silver behenate. The measurements were performed in vacuum with the exposure time of 10 s. The plot of intensity vs q were integrated in the cake slice of 30° along Q_z and Q_{xy} . The data was analyzed by SciAnalysis. (<http://gisaxs.com/index.php/SciAnalysis>)

Electrical conductivity and Seebeck coefficient measurements:

Sheet resistance was measured with a four-point probe setup (Signatone S302-4, Keithley 2450 source meter); film thicknesses were measured with a Dektak D6M/32 profilometer.⁸

A custom-built setup was used to check Seebeck coefficient (more information in our previously report).⁸ 100 nm bismuth (calibrated $\alpha = -62.1 \mu\text{V/K}$) and 50 nm of gold which work as the electrodes and electrical contact pads was thermally evaporated.

Optical absorbance:

UV-Vis absorbance spectra were measured with an Ocean Optics QE Pro high performance spectrometer; Raman spectra were measured with a thermo scientific DXR Smart-Raman. UV-Vis-NIR absorbance spectra were measured at normal incidence using a grating-type spectrophotometer in the photon energy regions of 0.5–3eV at room temperature. The absorption spectra are calculated using $\alpha(\omega) = -Ln\left(\frac{T(\omega)_{film+sub}}{T(\omega)_{sub}}\right)$.

Atomic Force Microscopy (AFM):

The samples were characterized using Park XE-70 Atomic Force Microscope.

CV measurements:

Cyclic voltammetric measurements were conducted in a single-compartment electrochemical cell with three electrodes: working electrode (glassy carbon, geometric area of 0.07 cm²), reference electrode (Ag/AgCl) and the counter electrode (Pt wire). Cyclic voltammetric (CV) curves were recorded by an electrochemical workstation (CHI-760D, CH Instruments, Austin, TX). For working electrode, an active material was cast on glassy carbon current collector. The electrochemical measurements were recorded after purging with N₂ for 10 min. 0.1 M tetrabutylammonium hexafluorophosphate in chloroform was used as the supporting electrolyte. All sample had a concentration of *ca.* 0.2 mM and were measured with a scan speed of 50 mV*s⁻¹.

Reference:

- (1) Mohapatra, S. K.; Zhang, Y.; Sandhu, B.; Fonari, M. S.; Timofeeva, T. V.; Marder, S. R.; Barlow, S. Synthesis, characterization, and crystal structures of molybdenum complexes of unsymmetrical electron-poor dithiolene ligands. *Polyhedron* **2016**, *116*, 88-95.
- (2) Dunbar, K. R.; Quillevéré, A. [Fe₂Cl₆]²⁻: A Discrete Form of Ferrous Chloride. *Angew. Chem. Int. Ed.* **1993**, *32*, 293-295.

- (3) Davison, A.; Holm, R.; Benson, R.; Mahler, W. Metal complexes derived from cis - 1, 2 - dicyano - 1, 2 - ethylenedithiolate and bis (trifluoromethyl) - 1, 2 - dithiete. *Inorg. Synth.*, **2007**, 10, 8-26.
- (4) Dai, A.; Zhou, Y.; Shu, A. L.; Mohapatra, S. K.; Wang, H.; Fuentes - Hernandez, C.; Zhang, Y.; Barlow, S.; Loo, Y. L.; Marder, S. R. Enhanced charge - carrier injection and collection via lamination of doped polymer layers p - doped with a solution - processible molybdenum complex. *Adv. Funct. Mater.* **2014**, 24, 2197-2204.
- (5) Zhao, Y.; Zhao, X.; Zang, Y.; Di, C.-a.; Diao, Y.; Mei, J. Conjugation-Break Spacers in Semiconducting Polymers: Impact on Polymer Processability and Charge Transport Properties. *Macromolecules* **2015**, 48, 2048-2053.
- (6) Schroeder, B. C.; Kurosawa, T.; Fu, T.; Chiu, Y. C.; Mun, J.; Wang, G. J. N.; Gu, X.; Shaw, L.; Kneller, J. W.; Kreouzis, T. Taming charge transport in semiconducting polymers with branched alkyl side chains. *Adv. Funct. Mater.* **2017**, 27, 1701973.
- (7) Boehm, A. M.; Wieser, J.; Butrouna, K.; Graham, K. R. A new photon source for ultraviolet photoelectron spectroscopy of organic and other damage-prone materials. *Org. Electron.* **2017**, 41, 9-16.
- (8) Liang, Z.; Boland, M. J.; Butrouna, K.; Strachan, D. R.; Graham, K. R. Increased power factors of organic-inorganic nanocomposite thermoelectric materials and the role of energy filtering. *J. Mater. Chem. A* **2017**, 5, 15891-15900.